



OPEN ACCESS

EDITED BY

Xavier Gaona,
Karlsruhe Institute of Technology (KIT),
Germany

REVIEWED BY

Tiziana Missana,
Medioambientales y Tecnológicas, Spain
Sarah Saslow,
Pacific Northwest National Laboratory
(DOE), United States
Erich Wieland,
Paul Scherrer Institut (PSI), Switzerland

*CORRESPONDENCE

J. Stietz,
✉ jastietz@uni-mainz.de
T. Reich,
✉ treich@uni-mainz.de

RECEIVED 28 July 2023

ACCEPTED 06 October 2023

PUBLISHED 02 November 2023

CITATION

Stietz J, Amayri S, Häußler V, Prieur D and Reich T (2023), Uptake of Pu(IV) by hardened cement paste in the presence of gluconate at high and low ionic strengths.
Front. Nucl. Eng. 2:1268767.
doi: 10.3389/fnuen.2023.1268767

COPYRIGHT

© 2023 Stietz, Amayri, Häußler, Prieur and Reich. This is an open-access article distributed under the terms of the [Creative Commons Attribution License \(CC BY\)](https://creativecommons.org/licenses/by/4.0/). The use, distribution or reproduction in other forums is permitted, provided the original author(s) and the copyright owner(s) are credited and that the original publication in this journal is cited, in accordance with accepted academic practice. No use, distribution or reproduction is permitted which does not comply with these terms.

Uptake of Pu(IV) by hardened cement paste in the presence of gluconate at high and low ionic strengths

J. Stietz^{1*}, S. Amayri¹, V. Häußler¹, D. Prieur² and T. Reich^{1*}

¹Department of Chemistry, Johannes Gutenberg-Universität Mainz, Mainz, Germany, ²Institute of Resource Ecology, Helmholtz-Zentrum Dresden-Rossendorf e.V., Dresden, Germany

The uptake of Pu(IV) by hardened cement paste (HCP) at degradation state I was investigated in the absence and presence of gluconate (GLU). Furthermore, the influence of the ionic strength was examined in different background electrolytes. Artificial cement pore water (ACW, pH = 13) was used for low ionic strength ($I = 0.3$ M), and cement pore water based on the diluted caprock solution (ACW-VGL, pH = 12.5) was used for high ionic strength ($I = 2.5$ M). Sorption experiments were performed under an Ar atmosphere using HCP in the HCP/GLU binary system ($[GLU]_0 = 1 \times 10^{-1} - 1 \times 10^{-8}$ M) and the HCP/Pu(IV)/GLU ternary system ($[^{239}\text{Pu(IV)}]_0 = 1 \times 10^{-8}$ M, $[GLU]_0 = 1 \times 10^{-2}$ M) with solid-to-liquid (S/L) ratios of 0.5–50 g L⁻¹ within a contact time of 72 h. GLU sorbs strongly on HCP; a saturation of the sorption sites of HCP with GLU was observed at $[GLU] \geq 1 \times 10^{-4}$ M at S/L = 5 g L⁻¹. The effects of the order of addition of the components Pu(IV) and GLU on the sorption of Pu(IV) on HCP were investigated. In the absence of GLU, a quantitative uptake ($S\% \geq 99\%$) of Pu(IV) by HCP was observed, independent of the ionic strength of the background electrolytes. In the presence of 1×10^{-2} M GLU, the sorption of Pu(IV) on HCP was significantly lower. For X-ray absorption fine structure (XAFS) measurements, powder samples with Pu ($[^{239}\text{Pu(III)}]_0 = 5 \times 10^{-6}$ M) sorbed on HCP (S/L = 2.5 g L⁻¹) were prepared at pH ≈ 13 in ACW and ACW-VGL, respectively. One additional sample was prepared in the presence of GLU ($[GLU]_0 = 1 \times 10^{-2}$ M) with ACW-VGL as the electrolyte for comparison. Pu L_{III}-edge X-ray absorption near-edge structure (XANES) spectra show that Pu is in the tetravalent oxidation state after being taken up by the HCP. The structural parameters obtained from extended X-ray absorption fine structure (EXAFS) analysis and comparison with literature indicate incorporation of Pu(IV) into the calcium-silicate-hydrate (C-S-H) phases of HCP. The different ionic strengths and the presence of GLU had no influence on the near-neighbor environment of Pu in HCP.

KEYWORDS

sorption, ionic strength, plutonium, ordinary Portland cement, gluconate, extended X-ray absorption fine structure, X-ray absorption near-edge structure

1 Introduction

The assessment of environmental issues regarding the long-term disposal of radioactive waste is essential in nuclear waste management. In a deep geological nuclear waste repository, cement-based materials will be used not only as a building material but also as a part of the engineered barrier, including waste containers and surrounding backfill

materials (Duro et al., 2020; Tyupina et al., 2023). Hydrated cement is the main component of concrete used in the repository. In this context, hydrated cement phases buffer the pH value, and thus three main states of cement degradation are described by the interaction with inflowing groundwater or pore water from the host rock of the repository. In the first state, the cement pore water evolves from a solution dominated by NaOH and KOH ($[Na] \approx 0.1$ M, $[K] \approx 0.2$ M, $pH \approx 13.3$) to a solution saturated with portlandite ($Ca(OH)_2$) with a pH of 12.5 (state II). After leaching of the portlandite, cement degradation achieves a third state characterized by the noncongruent dissolution of the calcium-silicate-hydrate (C-S-H) phases and a decrease of pH in the cement pore water to ≈ 10 (Ochs et al., 2016). Changes in cement chemistry, such as pH shifts or dissolution of cement phases, can affect radionuclide mobility and interactions and must, therefore, be included in risk assessments.

This investigation deals with degradation state I, where the cement is largely fresh ($pH > 12.5$). The composition of incoming groundwater varies in terms of ionic strength, depending on the specific location of the repository. For instance, in the clay formations of Northern Germany, a high ionic strength ($I = 2.5$ M) is expected due to the significant salt content, as described by the “Standortmodell NORD” (Lommerzheim and Jobmann, 2015; Jobmann et al., 2017). On the other hand, pore water in clay formations in Southern Germany typically exhibits a lower ionic strength ($I = 0.3$ M) (Jobmann and Lommerzheim, 2015). If the cement comes into contact with the pore water of the clay formation, degradation of cementitious materials can occur, potentially leading to significant changes in the geochemical environment in the near field of the repository (Duquette et al., 2009; Guo et al., 2020).

The present investigation on the influence of ionic strength on actinide retention is intended to provide information on the extent to which the findings obtained for low ionic strength also apply to the description of actinide retention at higher ionic strength. Furthermore, to be able to make statements about the safety of such a repository, it is necessary to investigate processes such as sorption of the actinides on cementitious materials. The radioactive waste will contain long-lived actinides, such as plutonium ($t_{1/2}^{(239}Pu) = 2.41 \times 10^4$ a). The isotope ^{239}Pu is present as a component of spent nuclear fuel and highly relevant in the long-term safety assessment of a deep geological radioactive waste repository. Strongly reducing conditions are expected in the repository in the case of anaerobic iron corrosion (e.g., steel containers) and hydrogen formation. Therefore, the actinides will be predominantly in oxidation states +III and +IV (Duro et al., 2014). In aqueous solutions, plutonium can be present in different oxidation states simultaneously. Under the reducing and hyperalkaline environment as a result of cement degradation, Pu(IV) is expected as the dominant species (Stietz et al., 2023). Only a few studies have examined the uptake of Pu(III/IV) on hardened cement paste (HCP), including Wieland (2014) and Ochs et al. (2016). Distribution ratios, R_d , up to 1×10^4 L kg⁻¹ were reported for cement by Ochs et al. (2016). Wieland et al. (2014) reported an R_d value of 10^5 L kg⁻¹ for An(IV) in the degradation states I–III. Tasi et al. (2021) reported an R_d value of 2×10^6 L kg⁻¹ for Pu(IV) uptake by HCP at degradation state II ($pH = 12.6$). Experiments by Häußler et al. (2018) with Pu(III) and C-S-H phases ($S/L = 5$ g L⁻¹; calcium-to-silicon ratio (Ca/Si) = 0.7–1.8) have shown an R_d value of 2×10^5 L kg⁻¹ but also showed that Pu(III) was oxidized to Pu(IV) during the uptake by C-S-H.

In addition, due to cement degradation, organic ligands present in the form of cement additives or degradation products of cellulose and other organic waste materials could affect the migration behavior of actinides in a cement-based repository (Altmaier et al., 2021). Some studies have examined the complexation of actinides with such organic ligands like EDTA, isosaccharinic acid (ISA), and gluconate (GLU) and their effect on the sorption of actinides on cementitious phases as well as changes of the structure and chemical composition of the C-S-H phases (Taylor, 1997; Tits et al., 2005; Dario et al., 2006; Glaus et al., 2006; Gaona et al., 2008; Altmaier et al., 2021; Ochs et al., 2022).

GLU is used as an organic additive in concrete formulations, and its interaction with cementitious phases was investigated, for example, by Androniuk et al. (2017). In the concentration range of 1×10^{-9} – 1×10^{-2} M GLU, an R_d value of 285 L kg⁻¹ was determined for the sorption of GLU on the C-S-H phase with Ca/Si = 1.4. This study also showed that GLU sorption is a fast process. The equilibrium was reached after only 1 day, which is also in agreement with results of Glaus et al. (2006). Furthermore, GLU forms stable complexes with Ca(II) occurring in cementitious systems (Kutus et al., 2020) and with a variety of radionuclides, due to its carboxyl group and hydroxyl groups, which can participate in complexation processes (Tits et al., 2005; Gaona et al., 2008; Colàs et al., 2013; Adam et al., 2021). The formation of aqueous ternary complexes with GLU and Ca(II) is reported for tri- and tetravalent actinides (Colàs et al., 2013; Böszörményi et al., 2020; Rojo et al., 2021).

In the HCP/Pu(IV)/GLU ternary system, Gaona et al. (2008) described a possible formation of a $Pu(IV)(OH)_4(GLU)^-$ complex as the predominant species observed under alkaline to hyperalkaline conditions in solution. Tits et al. (2005) determined an R_d value of 3×10^4 L kg⁻¹ for the sorption of Th(IV) on calcite in the presence of GLU. Tasi et al. (2021) investigated the interaction of Pu with cement at degradation state II in the presence of ISA as another representative of polyhydroxy carboxylic acids likely to be present in cementitious repositories. In the presence of ISA ($[ISA]_{tot} \geq 10^{-4.5}$ M) low uptake of Pu(IV) on cement was observed, which decreased with increasing ISA concentration.

To the best of our knowledge, no previous literature has been reported on sorption experiments and spectroscopic investigations specifically examining the Pu-GLU system in relation to cementitious materials. Consequently, the primary objective of this study was to explore the sorption behavior of Pu on HCP, in both the absence and presence of GLU. In addition, the influence of ionic strength was assessed by using two different electrolytes: artificial cement pore water (ACW, $I = 0.3$ M) and a diluted caprock solution based on artificial cement pore water (VGL, German acronym for *Verdünnte Gipshuttlösung*, ACW-VGL; $I = 2.5$ M). The third aim was to determine the oxidation state of Pu sorbed on HCP and to obtain molecular-level information about the effects of GLU and ionic strength on the Pu sorption using X-ray absorption fine structure (XAFS) spectroscopy.

2 Materials and methods

All experiments were performed under anaerobic conditions in a glove box under an Ar atmosphere ($Ar \geq 99.99\%$, $O_2 < 0.1$ ppm) to exclude oxidation processes by O_2 and to eliminate carbonate

complexation by dissolved CO₂. Solutions were prepared using Milli-Q water (18.2 MΩ cm, Synergy™ Millipore water system, Millipore GmbH, Germany) previously degassed with Ar. All chemicals used for the solutions were p. a. (pro analysis) quality grade or better. Furthermore, the production of HCP powder (particle size of $\varnothing < 63 \mu\text{m}$) from ordinary Portland cement (Dyckerhoff, Germany) with a water-to-cement ratio (w/c) of 0.5 was based on DIN EN 196–3 (DIN, 2009), which has been slightly modified as described in Stietz et al. (2023).

2.1 Stock solutions

2.1.1 Gluconate

For the experiments in the HCP/GLU binary system, a stock solution of 3.7 MBq mL⁻¹ ¹⁴C-GLU (Hartmann Analytic, Germany) was diluted to the desired concentration in Milli-Q water. Furthermore, an inactive GLU stock solution ([GLU] = 0.3 M) was prepared from sodium gluconate (Sigma-Aldrich, United States) in Milli-Q water.

2.1.2 Plutonium

After purification from its decay products and ²⁴¹Am using anion exchange chromatography, ²³⁹Pu(VI) stock solution was obtained by fuming it several times with 1 M HClO₄ (Riedel-de Haën, Germany) (not to complete dryness) (Amayri et al., 2016). The tri- and tetravalent oxidation states of Pu were obtained from the purified Pu(VI) stock solution by potentiostatic electrolysis using a potentiostat (Wenking POS 2, Bank Elektronik-Intelligent Controls GmbH, Germany) in 1 M HClO₄ using a three-electrode cell consisting of a Pt-mesh as a working electrode, a Pt counter-electrode separated from the cell by a Vycor frit, and an Ag/AgCl reference electrode following the methods described by Cohen (1961). The oxidation state was verified by UV-vis spectroscopy: (Tidas 100, J & M Analytik AG, Germany) using the characteristic absorption bands at 601 nm for Pu(III), 470 nm for Pu(IV), 569 nm for Pu(V), and 830 nm for Pu(VI) (Cohen, 1961). The concentration of the ²³⁹Pu stock solutions was determined by liquid scintillation counting (LSC; Hidex 300 SL, Hidex, Finland) and α -spectroscopy (Si surface barrier detector, CR-SNA-450–100, AMETEK, USA). An aliquot of the ²³⁹Pu stock solution was diluted in 1 M HClO₄ to achieve initial concentrations of 1×10^{-8} M Pu(IV) for batch experiments and 5×10^{-6} M Pu(III) for XAFS investigations, respectively.

2.2 Background electrolytes

2.2.1 Artificial cement pore water

Sorption batch experiments at low ionic strength were carried out using ACW with a composition of 0.18 M KOH (Merck, Germany) and 0.114 M NaOH (Merck, Germany), yielding a pH value of 13.3. This composition corresponds to the experimental results obtained according to Wieland et al. (2006). An ICP-MS SemiQuant analysis: (7900 Series ICP-MS, Agilent Technologies, United States) was performed to determine the chemical composition of ACW after a 72 h contact time with HCP (S/L = 5 g L⁻¹). The results of the measurement are summarized in Table 1. For more information, please refer to Supplementary Material S1.

2.2.2 Cement pore water based on diluted caprock solution

The diluted caprock solution (VGL) was chosen as a reference solution for the high ionic strength to simulate the prevailing conditions at the interface between neighboring claystone and salt formations in Northern Germany. ACW based on VGL (Meleshyn, 2015) was prepared via leaching of HCP powder in a VGL solution under an Ar atmosphere. For this, HCP powder (grain size < 63 μm , w/c = 0.5) was suspended in VGL (S/L = 10 g L⁻¹) and shaken for at least 1 week in an overhead shaker (Reax 20, Heidolph Instruments GmbH & Co. KG, Germany) at 16 rpm. To separate the solid and liquid phases, the wide-mouth bottles (Beckman Coulter, United States) were first centrifuged for 15 min at 7,000 rpm (7,519 g) with an Avanti J-30I (Beckman Coulter, United States). Subsequently, the supernatant was filtrated using a 50-mL syringe with a disposable syringe filter (CHROMAFIL® Xtra PVDF-20/25, pore size: 0.2 μm , filter- ϕ : 25 mm, Macherey-Nagel GmbH & Co. KG, Germany). The pH value of the ACW-VGL solution was 12.8. The individual constituents of VGL (Meleshyn, 2015) and ACW-VGL (determined with XRF) are listed in Table 1. The XRF measurement is given in Supplementary Material S2.

2.3 Batch experiments

The HCP powder was mixed with the related ACW or ACW-VGL background electrolyte to achieve suspensions with S/L ratios between 0.5 and 50.0 g L⁻¹. The samples were turned in an end-over-end rotator (Stuart Rotator SB3, United Kingdom) for a preconditioning period of 72 h. The individual experiments are described in more detail in Section 2.3.2. For phase separation, the samples were precentrifuged at 3,770 g (SIGMA 3K30, SIGMA Laborzentrifugen GmbH, Germany) for 15 min and ultracentrifuged at 108,800 g (Avanti J-30I, Beckman Coulter; United States) for 1 h. The pH value was measured in all samples immediately after centrifugation. The pH values in both electrolytes remained constant after a contact time of 72 h.

2.3.1 pH and Eh measurements

A pH meter (WTW inoLab. pH Level 1, WTW GmbH, Germany) equipped with a pH electrode (BlueLine 16 pH, Schott Instruments GmbH, Germany) was used for the measurement of the pH of the supernatant solutions. The electrode was calibrated regularly using certificated buffer solutions of pH 4.01, 6.87, and 9.18 (Schott Instruments GmbH, Germany). Samples at pH values in the high alkaline range were controlled with certificated buffer solutions of pH 13.00 (Hanna Instruments, Inc., United States). The measured pH value for this buffer was 12.89, giving an uncertainty of $\Delta\text{pH} = 0.11$ when using this calibration. It is necessary to correct the measured pH values obtained at higher ionic strengths because of the discrepancies between the activities of the ions in the electrolyte solution of the electrode and the sample solution (Fanghänel et al., 1996). An empirically derived correction parameter ($A = 0.41$) was used to accurately account for these differences according to the following equation (Fanghänel et al., 1996):

TABLE 1 Composition of the background electrolyte ACW (Wieland et al., 2006) and the result of the semiquantitative analysis made in ICP-MS of ACW after 72 h contact time with HCP (S/L = 5 g L⁻¹). For the preparation of the background electrolyte with high ionic strength, the composition of VGL (Meleshyn, 2015) and the results from the XRF analysis of ACW-VGL after 10 days of contact time with HCP (S/L = 10 g L⁻¹) are summarized.

	Concentration/M			
	ACW (Wieland et al., 2006)	ACW ^a	VGL (Meleshyn, 2015)	ACW-VGL ^b
Na ⁺	0.11	0.14	2.52	2.40
K ⁺	0.18	0.22	5.0 × 10 ⁻³	3.6 × 10 ⁻³
Ca ²⁺	-	2.8 × 10 ⁻³	1.00 × 10 ⁻²	2.03 × 10 ⁻²
Cl ⁻	-	-	2.52	1.86
SO ₄ ²⁻	-	2.0 × 10 ⁻³	8.0 × 10 ⁻³	3.8 × 10 ⁻⁴
Si ⁴⁺	-	4.3 × 10 ⁻⁴	-	1.2 × 10 ⁻³
pH	13.3	13.3	8.0	12.8
IS/M	0.3	0.3	2.6	2.5

^aObtained from ICP-MS SemiQuant analysis, Supplementary Table S1.

^bObtained from XRF analysis, Supplementary Table S2.

$$pH = pH_{exp} + A. \quad (1)$$

The redox potentials were determined using a pH meter connected with a redox electrode (BlueLine 31 RX, reference system: Ag/AgCl, Schott Instruments GmbH, Germany). To ensure the accuracy and reliability of the setup, the functionality was verified using standard solutions of known potentials (+220 mV, +470 mV, and +640 mV; Schott Instruments GmbH, Germany). All values were converted to the standard hydrogen electrode (SHE) by adding 210 mV to the measured values.

2.3.2 Sorption experiments

2.3.2.1 HCP/GLU

The uptake of GLU by HCP was investigated in two different series of batch experiments after a contact time of 72 h. The contact time of 72 h was considered sufficient because a rapid uptake process of GLU was shown in the literature, where the equilibrium was reached after only 1 day (Glaus et al., 2006; Androniuk et al., 2017). One batch experiment was performed as a function of the S/L ratio ([GLU]₀ = 1 × 10⁻² M; S/L = 0.5–50 g L⁻¹) and the other as sorption isotherm of GLU (S/L = 5 g L⁻¹; [GLU]₀ = 1 × 10⁻⁹–1 × 10⁻¹ M). In both experiments, ¹⁴C-labelled GLU (2.5–200 Bq ¹⁴C-GLU) was used as a tracer and analyzed by LSC. A 1–2 mL sample was added to 10 mL LSC cocktail Ultima Gold™ XR (PerkinElmer LAS GmbH, Germany) without acidifying. Samples were measured until a 2σ error of 2% was achieved. The resulting limit of detection (LOD) for ¹⁴C-GLU was 1 × 10⁻⁹ M.

2.3.2.2 HCP/Pu(IV)

Sorption batch experiments in the HCP/Pu(IV) binary system after a contact time of 72 h aimed to provide a basis for interpreting the Pu uptake in the presence of GLU at high and low ionic strengths using different approaches. Each sample was prepared in duplicate. In the first batch experiment, the sorption of Pu(IV) ([²³⁹Pu(IV)]₀ = 1 × 10⁻⁸ M) on HCP was determined with ICP-MS analysis (7900 Series ICP-MS, Agilent Technologies, United States).

After phase separation, the supernatant was diluted in 2% HNO₃. ¹⁹³Ir ([Ir] = 100 ppt) in 2% HNO₃ was added as an internal standard. The LOD for ICP-MS measurements of ²³⁹Pu was 2 × 10⁻¹⁰ M.

The measured concentration [Pu]_{eq} [M] of the analyte in the supernatant and its initial concentration [Pu]₀ [M], respectively, were used to calculate the sorption:

$$Sorption\% = \left(1 - \frac{[Pu]_{eq}}{[Pu]_0}\right) \cdot 100\%. \quad (2)$$

The distribution ratio R_d [L kg⁻¹] between the solid and the liquid phases was calculated using Eq. (3), with the sample volume V [L] and the total mass of the solids m [kg]:

$$R_d = \frac{V}{m} \cdot \left(\frac{[Pu]_0 - [Pu]_{eq}}{[Pu]_{eq}}\right). \quad (3)$$

2.3.2.3 HCP/Pu(IV)/GLU

In order to study the influence of GLU as an organic additive on the sorption behavior, experiments in the HCP/Pu(IV)/GLU ternary system were performed. The order of addition of Pu(IV) ([Pu]₀ = 1 × 10⁻⁸ M) and GLU ([GLU]₀ = 1 × 10⁻² M) on HCP (S/L = 5 g L⁻¹) was varied in three combinations: (i) (HCP + Pu(IV)) + GLU, Pu(IV) was equilibrated with HCP for 72 h, followed by the addition of GLU, also with a contact time of 72 h. In variation (ii), described as (HCP + GLU) + Pu(IV), GLU was equilibrated with HCP for 72 h before the addition of Pu(IV) and subsequently equilibrated for 72 h. In variation (iii), (HCP + Pu(IV) + GLU), GLU and Pu(IV) were added simultaneously and equilibrated for 72 h. Each sample was prepared in duplicate.

2.3.3 XAFS measurements of ²³⁹Pu

To examine the sorbed Pu species after the uptake by HCP at different ionic strengths, samples were prepared in the background electrolytes ACW and ACW-VGL with an initial concentration of 5 × 10⁻⁶ M ²³⁹Pu(III) as described in Section 2.3.2.2 (HCP/Pu(IV)).

TABLE 2 Samples of the Pu/HCP binary and the Pu/HCP/GLU ternary systems prepared for Pu L_{III}-edge XAFS measurements with S/L = 2.5 g L⁻¹ and an initial concentration of 5 × 10⁻⁶ M Pu(III).

Sample	[GLU] ₀ /M	pH	Pu/ppm
Pu/HCP in ACW	-	13.4	493
Pu/HCP in ACW-VGL	-	12.3	493
Pu/HCP/GLU in ACW-VGL	0.01	12.7	479

The influence of 1 × 10⁻² M GLU was investigated by preparing one additional sample in ACW-VGL, where aliquots of Pu(III) and GLU stock solutions were added simultaneously to the pre-equilibrated HCP suspension. To increase the uptake of Pu by HCP for the spectroscopic measurements, the S/L ratio during sample preparation was reduced to 2.5 g L⁻¹. A description of the samples can be found in Table 2. The samples were prepared using Pu(III) because its hydrolysis is less and its solubility is higher than Pu(IV) (Grenthe et al., 2020). Therefore, the initial concentration could be increased, which was necessary to perform these spectroscopic investigations. In addition, the use of Pu(III) prevented the formation of Pu(IV) colloids and solid phases (PuO_{2(hyd,aged)}) at the high pH. After centrifugation of the samples, the solid phase was dried under an Ar atmosphere at room temperature, homogenized, and transferred into double-confinement oblong plastic holders transparent to X-rays. The samples were transported under a liquid nitrogen atmosphere to the European Synchrotron Radiation Facility (ESRF), Grenoble, France. Synchrotron radiation XAFS measurements of the batch samples were performed in 7/8 bunch mode at the BM20 Rossendorf Beamline (ROBL) (Matz et al., 1999; Scheinost et al., 2021) using the Si(111) double-crystal monochromator. Higher harmonic radiation was rejected by Rh-coated mirrors positioned in front of and behind the monochromator. During the measurements, the samples were cooled to 15 K with a closed-cycle He cryostat (CryoVac, Germany). A 13-element Ge-detector (Canberra, United States) was used to record multiple scans of the Pu L_{III}-edge XAFS spectrum in fluorescence mode. During each scan, the Zr K-edge spectrum of a Zr foil was measured simultaneously in transmission mode. The corresponding ionization chambers were filled with a gas mixture of 82% N₂ and 18% Ar. The X-ray absorption near-edge structure (XANES) spectra of the Zr K-edge (17,998 eV) and the Pu L_{III}-edge (18,057 eV) were recorded with a step size of 0.5 eV. The extended X-ray absorption fine structure (EXAFS) part of the Pu spectrum was recorded in *k*-space with a step size of 0.05 Å⁻¹ and a gradually increasing counting time from 2 s to 20 s per data point. The programs EXAFSPAK (George and Pickering, 2000) and FEFF9 (version 9.6) (Rehr et al., 2010) were used to analyze the EXAFS spectra. A structural model based on density functional calculations of the sorption modes of U(IV) at the C-S-H phase (Chiorescu et al., 2022), where the U in the CaO layer of C-S-H was replaced by Pu, was used for the calculation of the FEFF scattering amplitudes and phases.

The recorded XANES spectra were analyzed using the software package Demeter, Athena, v. 0.9.025 (Ravel and Newville, 2005). After energy calibration using the Zr K-edge energy at 17,998 eV, the

spectra were averaged and modeled using least-squares fitting and the reference spectra of Pu(III) aquo ion (Schmeide et al., 2006) and PuO₂ (Martin et al., 2007). In addition, the energy of the Pu L_{III} edge in the XANES spectra of the HCP samples was determined based on the first inflection point, which is defined as the zero-crossing of the second derivative of the XANES.

3 Results and discussion

3.1 Sorption experiments

3.1.1 HCP/GLU

As described in Section 2.3.2.1, the uptake of GLU by HCP at degradation state I was investigated with ¹⁴C-labelled GLU as the sorption isotherm (Figure 1A) and as a function of the S/L ratio (Figure 1B). In Figure 1A, the values flatten at [GLU]₀ ≥ 1 × 10⁻⁴ M, indicating saturation of the HCP sorption sites. Below this concentration, that is, the range relevant for the waste repository, the sorption isotherm is linear and has a slope of 1. The *R_d* value equals (4.9 ± 0.4) × 10³ L kg⁻¹. All data of the GLU/HCP system were modeled using the two-site Langmuir isotherm given in Eq. (4):

$$[\text{GLU}]_{\text{sorbed}} = \frac{K_1 q_1 [\text{GLU}]_{\text{eq}}}{1 + K_1 [\text{GLU}]_{\text{eq}}} + \frac{K_2 q_2 [\text{GLU}]_{\text{eq}}}{1 + K_2 [\text{GLU}]_{\text{eq}}}, \quad (4)$$

where *K*_{1,2} [L mol⁻¹] is the adsorption affinity constant, *q*_{1,2} [mol kg⁻¹] is the sorption capacity of HCP for GLU for two distinct sorption sites, and [GLU]_{eq} is the equilibrium concentration. The Langmuir isotherm parameters for both background electrolytes are summarized in Table 3. These parameters were used to calculate the equilibrium concentration [GLU]_{eq} as a function of S/L for [GLU]₀ = 1 × 10⁻² M using Eq. (5). The calculated concentrations [GLU]_{eq} agree well with the experimental data as shown in Figure 1B.

$$[\text{GLU}]_{\text{sorbed}} = ([\text{GLU}]_0 - [\text{GLU}]_{\text{eq}}) \times \frac{V}{m}. \quad (5)$$

In general, as the amount of HCP in solution increased to 50 g L⁻¹, the equilibrium concentration of GLU in solution decreased for both electrolytes. Particularly in the range between 5 and 20 g L⁻¹, the equilibrium concentration differs regarding the ionic strength of the background electrolytes. The exact distribution of the ligand on the sorption sites cannot be deduced. One possibility would be the uptake of GLU into the interlayer of the C-S-H phase. Due to the high affinity of GLU to Ca²⁺ and its H-bonding ability, a strong interaction of GLU with the cement surface is expected (Pallagi et al., 2014; Kutus et al., 2020). According to the calculated speciation (see Supplementary Material S3, Supplementary Figure S1), Ca-GLU complexes are formed under the experimental conditions. Due to a higher Ca²⁺ concentration in ACW-VGL (Table 1), proportionally more [Ca(OH)(GLU)]_{aq} is formed, which may not sorb onto the HCP surface. This could lead to a lower uptake of GLU by HCP in ACW-VGL and a higher GLU concentration in solution, as seen in Figure 1B, respectively. At low S/L ratios (S/L ≤ 2 g L⁻¹), the amount of GLU is probably so high that the influence of the background electrolyte is not significant. At an S/L ratio of

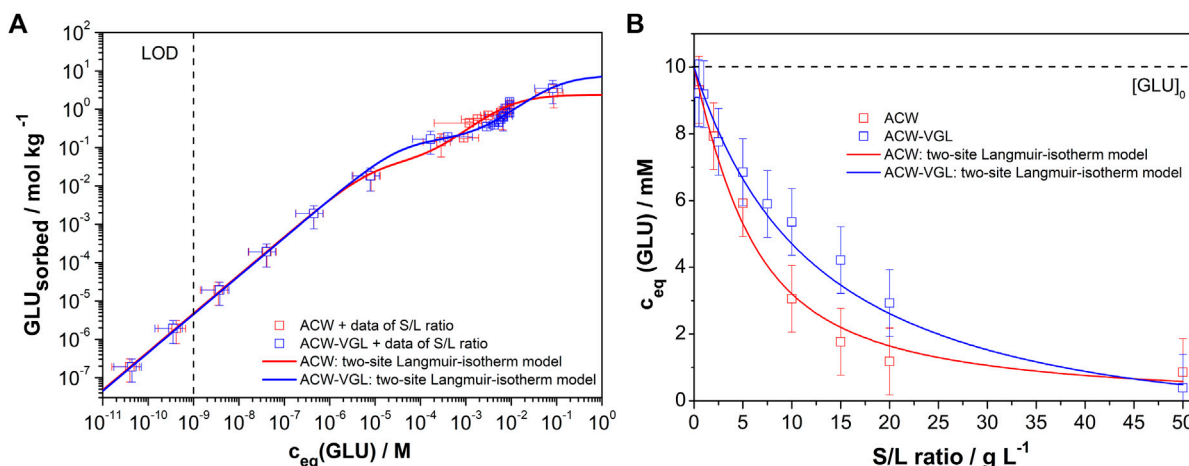


FIGURE 1
 Batch sorption experiments of GLU at HCP with ACW (red, pH = 13.3) and ACW-VGL (blue, pH = 12.8) and a contact time of 72 h: (A) sorption isotherm with initial GLU concentrations from 1×10^{-9} M to 1×10^{-1} M at $S/L = 5 \text{ g L}^{-1}$. The dashed black line shows the limit of detection (LOD); (B) at constant GLU concentration ($[GLU]_0 = 1 \times 10^{-2}$ M) and varying S/L ratio ($S/L = 0.5\text{--}50 \text{ g L}^{-1}$). The dashed black line marks the initial concentration of 1×10^{-2} M GLU. The solid red and blue lines in (A) represent the best fit using two-site Langmuir sorption isotherms. The colored lines in B are the equilibrium concentrations of GLU calculated using Eq. 5 with the parameters in Table 3.

TABLE 3 Sorption affinity constants K_1 and K_2 and sorption capacities q_1 and q_2 for two distinct sorption sites determined by fitting the GLU sorption data using a two-site Langmuir sorption isotherm.

Langmuir-isotherm parameter	GLU/HCP in ACW	GLU/HCP in ACW-VGL
K_1/mol^{-1}	$(1.1 \pm 0.6) \times 10^5$	$(2.7 \pm 0.7) \times 10^4$
$q_1/\text{mol kg}^{-1}$	0.04 ± 0.02	0.16 ± 0.04
K_2/mol^{-1}	116 ± 39	11 ± 8
$q_2/\text{mol kg}^{-1}$	2.4 ± 0.5	7.5 ± 4.5

50 g L^{-1} , the concentration values converge again. The high uptake of GLU in both experiments is in good agreement with Androniuk et al. (2017) for C-S-H phases at a Ca/Si ratio of 1.4, which is representative of the Ca/Si ratio of C-S-H phases in unaltered HCP. Based on these results compared with the results from the literature (Androniuk et al., 2017), a blocking of sorption sites by GLU on HCP can be assumed.

3.1.2 HCP/Pu(IV)

First, the sorption of 1×10^{-8} M Pu(IV) on HCP ($S/L = 5 \text{ g L}^{-1}$) was studied in both background electrolytes. For the experiments, values of $R_{d,min} = 30 \text{ L kg}^{-1}$, $R_{d,max} = 8.5 \times 10^4 \text{ L kg}^{-1}$ (ACW), and $R_{d,max} = 2.4 \times 10^5 \text{ L kg}^{-1}$ (ACW-VGL) were determined as described in Tits et al. (2002). The results of the batch experiments show a high uptake of Pu by HCP independent of the ionic strength (see Table 4; R_d (ACW) = $1.3 \times 10^7 \text{ L kg}^{-1}$ ($S/L = 1 \text{ g L}^{-1}$) and $2.2 \times 10^6 \text{ L kg}^{-1}$ ($S/L = 5 \text{ g L}^{-1}$); R_d (ACW-VGL) = $2.6 \times 10^6 \text{ L kg}^{-1}$ ($S/L = 5 \text{ g L}^{-1}$)), which is in good agreement with the literature ($R_d > 10^4 \text{ L kg}^{-1}$ (Ochs et al., 2016) and $2.0 (+7.9/-0.5) \times 10^6 \text{ L kg}^{-1}$ (Tasi et al., 2021)). Furthermore, the speciation calculations for Pu indicate the species of $\text{Pu}(\text{OH})_4$ to be present over a wide pH range. Figure 2A shows the predominance diagram of Pu calculated

for an equilibrium concentration of $[\text{Pu}]_{eq} = 5 \times 10^{-8}$ M for both background electrolytes using the “Thermodynamic database ThermoChimie 9b0, 2015” (used complex formation constants are in SM-4). The measured Eh and pH values of the batch sorption samples, including those for the XAFS experiments, show that the samples are in the stability range of Pu(IV) (see Figure 2). Therefore, we assume that Pu(IV) is the species sorbed on the cement.

3.1.3 HCP/Pu(IV)/GLU

To our knowledge, no data are available for the uptake of Pu(IV) by HCP in the HCP/Pu(IV)/GLU ternary system. Table 4 summarizes the R_d values obtained from batch experiments where the order of addition was varied. These values are up to five orders of magnitude lower than those observed for the HCP/Pu(IV) binary system. The order of addition of Pu(IV) and GLU has a significant influence on the Pu uptake. When Pu(IV) was added first ($(\text{HCP} + \text{Pu}(\text{IV})) + \text{GLU}$), the corresponding distribution ratios are R_d (ACW) = $1.1 (\pm 0.1) \times 10^3 \text{ L kg}^{-1}$ and R_d (ACW-VGL) = $2.7 (\pm 0.4) \times 10^3 \text{ L kg}^{-1}$. In this case, GLU was added to the HCP suspension 72 h after the addition of Pu(IV). We assume that part of the Pu initially sorbed on HCP (compared with the binary system) was desorbed due to a mobilizing effect of

TABLE 4 Values for R_d , $R_{d,max}$ and $R_{d,min}$ in the experiments of the Pu(IV)/HCP binary system and the Pu(IV)/HCP/GLU ternary system under alkaline conditions (pH = 12.5–13) at high and low ionic strengths. Other parameters were $S/L = 5 \text{ g L}^{-1}$, $[\text{Pu(IV)}]_0 = 1 \times 10^{-8} \text{ M}$, $[\text{GLU}]_0 = 1 \times 10^{-2} \text{ M}$, and 72 h contact time.

Medium	Experiment	$R_d/\text{L kg}^{-1}$	$R_{d,max}/\text{L kg}^{-1}$	$R_{d,min}/\text{L kg}^{-1}$
ACW	HCP + Pu(IV)	2.2×10^6	8.5×10^4	
		1.3×10^{7a}	4.2×10^{5a}	
ACW-VGL	HCP + Pu(IV)	2.6×10^6	2.4×10^5	
Tasi et al. (2021)	HCP + Pu(IV)	$2.0 (+7.9/-0.5) \times 10^6$		
Ochs et al. (2016)	HCP + Pu(IV)	$> 10^4$		
ACW	(HCP + Pu(IV)) + GLU	$1.1 (\pm 0.1) \times 10^3$	6.3×10^5	
	(HCP + GLU) + Pu(IV)	0		30
	(HCP + Pu(IV) + GLU)	0		30
ACW-VGL	(HCP + Pu(IV)) + GLU	$2.7 (\pm 0.4) \times 10^3$	2.4×10^5	
	(HCP + GLU) + Pu(IV)	11 ± 6		30
	(HCP + Pu(IV) + GLU)	64 ± 30		30

^a) In this batch experiment, S/L was 1 g L^{-1} .

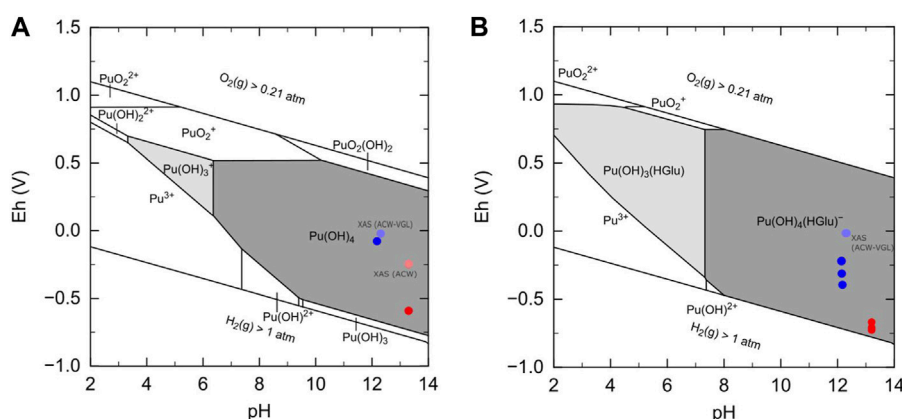


FIGURE 2

Speciation calculation for $5 \times 10^{-8} \text{ M}$ Pu in the absence (A) and the presence (B) of $1 \times 10^{-2} \text{ M}$ GLU. The dots mark the measured Eh (SHE) and pH values of the samples of the ACW-VGL (blue) and ACW (red) experiments. (Graphic generated by PhreePlot (version 1.0 (Parkhurst and Appelo, 2016)) using PHREEQC and the ThermoChimie database 9b0, 2015 (Giffaut et al., 2014)).

GLU. The desorption of Pu by GLU may be due to GLU being strongly taken up by HCP or to the complexation of Pu(IV) with dissolved GLU, as can be seen in the predominance diagram in Figure 2B. The measured Eh and pH values of all samples are in the predominance region of $\text{Pu(OH)}_4(\text{GLU})^-$ complex formation. Furthermore, no Pu uptake ($R_{d,min} = 30 \text{ L kg}^{-1}$) was observed when GLU was added first or simultaneously with Pu(IV) at low ionic strength (ACW). Also, small R_d values were determined (Table 4) at high ionic strength (ACW-VGL). In the second variant ((HCP + GLU) + Pu(IV)), GLU, which could be taken up at the HCP, was added first, so relevant sorption sites could be occupied, and Pu(IV) is not taken up at the HCP. Both components were added simultaneously in the third variant (HCP + Pu(IV) + GLU). Two effects could be important: first, the strong sorption of GLU on the HCP surface, and second, the formation of the $\text{Pu(OH)}_4(\text{GLU})^-$ complex that could remain in

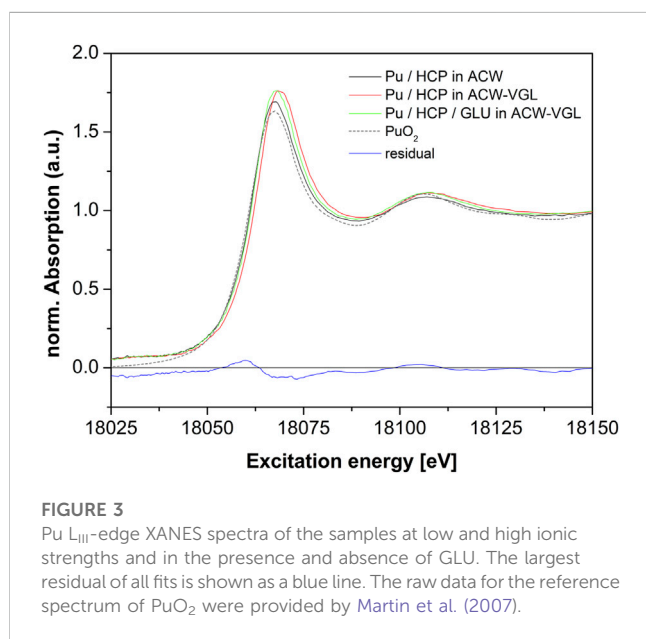
solution. The higher proportion of Ca^{2+} in ACW-VGL may be the reason for a slightly higher Pu uptake in ACW-VGL ($R_d = 64 \pm 30 \text{ L kg}^{-1}$) compared to the uptake in ACW (Table 4). Moreover, the comparison of the results for variant (i) with the other two variants indicates: (1) the sorption of Pu(IV) on HCP (variant (i)) may be partially irreversible. (2) The kinetics of Pu desorption from HCP by GLU are slower than its contact time of 72 h.

3.2 XAFS measurements (XANES and EXAFS)

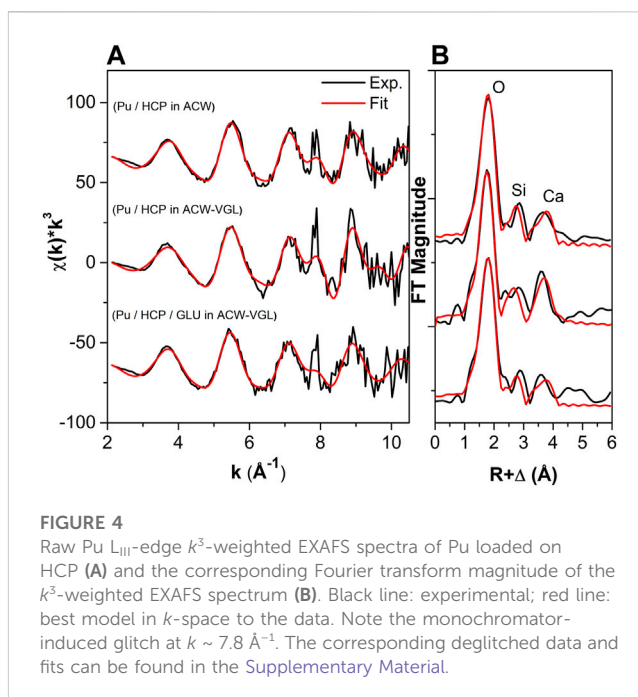
EXAFS measurements provide element-specific, short-range structural and chemical information on the Pu coordination environment, including identities and coordination numbers of the neighboring atoms and bond distances. We used this technique to obtain the local coordination environment of $5 \times$

TABLE 5 The Pu L_{III}-edge energies were determined by analyzing the inflection points of the XANES spectra of the samples studied. A comparison was made with the Pu(III)_(aq) and Pu(IV)_(aq) aquo ions (Conradson et al., 2004).

Absorption edges of Pu L _{III} -edge XANES	Energy/eV
Pu/HCP in ACW	18,062.8 (±0.6)
Pu/HCP in ACW-VGL	18,062.8 (±0.6)
Pu/HCP/GLU in ACW-VGL	18,062.6 (±0.7)
Pu(III) _(aq)	18,060.0
Pu(IV) _(aq)	18,063.2



10⁻⁶ M Pu after being taken up by HCP (S% = 99%, S/L = 2.5 g L⁻¹) in the investigated samples at high pH and in different electrolytes. The higher uptake of Pu in the presence of GLU (S% = 97%; [GLU]₀ = 1 × 10⁻² M) in this experiment can probably be attributed to the higher initial Pu concentration used. All samples were measured at approximately 15 K to reduce thermal vibrations and to enhance the corresponding contribution of these atoms to the EXAFS amplitude. Furthermore, the oxidation state of Pu retained on the HCP was investigated with Pu L_{III}-edge XANES spectroscopy. The energies of the absorption edges for the measured samples and of Pu(III)_(aq) and Pu(IV)_(aq) reference spectra (Conradson et al., 2004) are listed in Table 5. Additionally, a linear combination fit was performed using a subroutine in the program Athena (Ravel and Newville, 2005) to determine the fractions of different Pu oxidation states. This determination was achieved by fitting the measured XANES spectrum with reference spectra of Pu(III) aquo ion (Schneide et al., 2006) and PuO₂ (Martin et al., 2007) in the energy range between 18,012 and 18,212 eV. The Pu L_{III}-edge XANES spectra (Figure 3) demonstrate that Pu(IV) exclusively dominates as the oxidation state (100%) in the absence and presence of GLU. The relative uncertainty of the XANES fits with Pu(III) and Pu(IV) was less than 3%. The initial Pu(III) was oxidized to Pu(IV) after being taken up by the HCP. This solid phase characterization result



confirms the conclusion derived from the measured Eh and pH values of the supernatant solutions and the calculated predominance diagrams (Figure 2).

Figure 4 shows the raw Pu L_{III}-edge k³-weighted EXAFS spectra together with the best model to the data and the corresponding Fourier transform magnitudes for the samples Pu/HCP in the different background electrolytes and in the presence of GLU. The EXAFS spectra of the samples show similar oscillations, indicating similar Pu near-neighbor surroundings. Unfortunately, a monochromator-induced glitch between 18,284.6 eV and 18,299.9 eV (five measurement points) led to a distortion at k ~ 7.8 Å⁻¹ in the EXAFS spectra. An attempt to remove this glitch and to model the modified data can be found in Supplementary Material SM-7. The raw EXAFS data (Figure 4) were analyzed in k-space (2.1–10.9 Å⁻¹) without a window function and could be best modeled with three coordination shells. The total number of independent fit parameters was 10. The EXAFS structural parameters are summarized in Table 6. In the samples, Pu is surrounded by 6.0–6.7 (±0.4) oxygen atoms with Pu-O distances between 2.25 and 2.28 (±0.02) Å. These average Pu-O bond lengths agree with literature data for tetravalent Pu (Reich et al., 2007) and support the conclusion derived from the XANES measurements mentioned before. The second Pu coordination shell was modeled with Si. The average Pu-Si distance is between 3.15 and 3.16 (±0.02) Å, with Si coordination numbers between 1.1 and 1.8 (±0.6). The third coordination shell could be modeled as a Pu-Ca interaction with an average distance of 4.16–4.19 (±0.02) Å. For this coordination shell, a strong correlation between coordination number N and the Debye–Waller factor σ² was observed. For the samples Pu/HCP in ACW and Pu/HCP/GLU in ACW-VGL, the Ca coordination numbers are 5.2 ± 1.4 and 6.0 ± 2.3, respectively. For the Pu/HCP in the ACW-VGL sample, the Ca coordination number is lower, that is, 2.9 ± 0.9. Note that the corresponding σ² = 0.003 ± 0.002 is very small for such a distant shell. It should further

TABLE 6 Structural parameters of the Pu samples determined by Pu L_{III} -edge EXAFS spectroscopy with N - coordination number, R - distance, and σ^2 - Debye–Waller factor ($S_0^2 = 0.9$) and data from the literature for comparison.

Sample	Shell	N	$R/\text{\AA}$	$\sigma^2/\text{\AA}^2$
Pu/HCP/ACW (norm. error = 0.3, $\Delta E_0 = 1.5 \pm 0.4$ eV)	Pu-O	6.4 ± 0.3	2.27 ± 0.01	0.010 ± 0.001
	Pu-Si	1.4 ± 0.4	3.15 ± 0.01	0.005 ± 0.002
	Pu-Ca	5.2 ± 1.4	4.19 ± 0.01	0.011 ± 0.003
Pu/HCP/ACW-VGL (norm. error = 0.5, $\Delta E_0 = -1.1 \pm 0.7$ eV)	Pu-O	6.0 ± 0.4	2.25 ± 0.01	0.009 ± 0.001
	Pu-Si	1.8 ± 0.6	3.15 ± 0.01	0.007 ± 0.002
	Pu-Ca	2.9 ± 0.9	4.16 ± 0.01	0.003 ± 0.002
Pu/HCP/GLU/ACW-VGL (norm. error = 0.4, $\Delta E_0 = 1.1 \pm 0.5$ eV)	Pu-O	6.7 ± 0.4	2.28 ± 0.01	0.011 ± 0.001
	Pu-Si	1.1 ± 0.5	3.16 ± 0.01	0.006 ± 0.003
	Pu-Ca	6.0 ± 2.3	4.18 ± 0.01	0.015 ± 0.004
C-S-H (Ca/Si 1.65)/Pu/Milli-Q (pH = 12.5) (Stietz et al., 2023) (norm. error = 0.3, $\Delta E_0 = 1.31 \pm 0.4$ eV)	Pu-O	6.0 ± 0.3	2.27 ± 0.01	0.008 ± 0.001
	Pu-Si	1.2 ± 0.4	3.13 ± 0.01	0.006 ± 0.002
	Pu-Ca	5.0 ± 1.3	4.17 ± 0.01	0.011 ± 0.002

be noted that similar EXAFS structural parameters were obtained using the deglitched, k^3 -weighted EXAFS spectra (see Supplementary Table S4), with only one exception for sample Pu/HCP/GLU in ACW-VGL. Here, both N and σ^2 are strongly correlated and increased to 11.7 ± 5 atoms and $0.027 \pm 0.006 \text{ \AA}^2$, respectively. In addition, no Pu–Pu interaction could be modeled, indicating the absence of Pu clusters or precipitates at the HCP surface. Because both the atomic distances between Pu and its neighboring O, Si, and Ca atoms and the corresponding coordination numbers are almost identical for the three samples, one can conclude that neither ionic strength nor GLU affects the Pu uptake mechanism. No formation of ternary Pu(IV) complexes on HCP involving GLU was observed.

The obtained EXAFS structural parameters can be compared with previous EXAFS studies of Pu(IV) interaction with C-S-H (Ca/Si = 1.65, pH 12.5) (Stietz et al., 2023) and of Np(IV) interaction with HCP in ACW at pH 13.3 and with C-S-H (Ca/Si = 1.65, pH 12.5) (Gaona et al., 2011). For Pu/C-S-H, the following interatomic distances with coordination numbers in parentheses were reported: Pu-O 2.27 \AA (6), Pu-Si 3.13 \AA (1), and Pu-Ca 4.17 \AA (5) (see Table 6). These EXAFS structural parameters are very similar to those of the HCP samples of this study, indicating that C-S-H is the main phase responsible for the uptake of Pu(IV) by HCP.

Gaona et al. (2011) obtained the following interatomic distances with coordination numbers in parentheses for Np/C-S-H: Np-O 2.31 \AA (8.3), Np-Si 3.60 \AA (2.9), and Np-Ca 4.18 \AA (12.7). These results show some agreement and some differences compared to our Pu/HCP samples, that is, a longer Np-Si distance and a higher Ca coordination number. Based on a detailed discussion of the results, Gaona et al. concluded that “Np(IV) is incorporated in the interlayer of the C-S-H structure”.

The uptake of U(IV) by 14 \AA tobermorite (Ca/Si = 1.0) was investigated in a recent density functional calculation (Chiorescu et al., 2022). The quantum mechanical calculations of geometry

parameters and relative energies included U(IV) adsorption on the (001) surface, absorption in the interlayer, and incorporation into the CaO layer of tobermorite that served as a structural model for C-S-H. The results show that the structural parameters of the U-O coordination shell are insensitive to the different sorption mechanisms. Furthermore, the wide scatter of calculated U-Si distances between 3.0 and 4.2 \AA for all sorption modes makes it difficult to distinguish between them. The most promising parameter is the number of Ca atoms below 5.0 \AA . N is in the range of 2–4 for the thermodynamically most stable U(IV) complexes at the (001) surface and in the interlayer. For U(IV) incorporation into the CaO layer, the calculations yielded six Ca atoms between 3.7 – 4.2 \AA . Based on the close match between this DFT result and previous EXAFS measurements for Pu(IV)/C-S-H (Ca/Si = 0.8), it was concluded that incorporation of Pu(IV) into the CaO layer of C-S-H is the most probable uptake mechanism (Chiorescu et al., 2022; Dettmann et al., 2023). Compared to these quantum mechanical and spectroscopic results and taking into account the large uncertainty of coordination numbers determined by EXAFS, the uptake into the CaO layer of HCP might be the dominant but not the only uptake mechanism.

4 Conclusion

The results provide an improved basis for predicting the behavior of Pu in radioactive waste repositories under reducing conditions, independent of the ionic strength of the groundwater. The sorption experiments in the binary system show a quantitative uptake of Pu(IV) by HCP that is in good agreement with the sorption data available in the literature. The uptake of GLU by HCP could lead to saturation of the sorption sites and is also consistent with the sorption data available in the literature for C-S-H phases (Ca/Si = 1.4) (Androniuk et al., 2017).

The XANES measurements show that Pu(IV) is the predominant species after being taken up by HCP. The evaluation of the EXAFS measurements suggests that Pu is incorporated into the C-S-H phases, which are the main sorption phase of the HCP. Furthermore, the influence of the ionic strength was investigated, and neither it nor the presence of GLU showed an effect on the uptake of Pu by HCP.

The results show a significant influence of high GLU concentration ($[GLU]_0 = 1 \times 10^{-2} \text{ M}$) on the uptake of Pu(IV), independent of the ionic strength of the groundwater. The impact of the order of addition of Pu and GLU to HCP was investigated. The uptake of Pu by HCP in the presence of GLU decreases. Significant differences in the uptake are found in the experiments of (ii) (HCP + GLU) + Pu(IV) and (iii) (HCP + Pu(IV) + GLU), where (almost) no sorption occurred. This might be a competitive reaction of Pu(IV) and GLU, where GLU may have a desorbing effect or a complex of $\text{Pu}(\text{OH})_4(\text{GLU})^-$ might be formed. In addition, the amount of Ca^{2+} in the background electrolyte is crucial for the results of the experiments with GLU and, consequently, in the uptake of Pu by HCP. However, a significantly lower GLU concentration ($[GLU]_0 = 1 \times 10^{-8} \text{ M}$) is to be expected in a repository. A speciation calculation (see SM-5, Supplementary Figure S2) for this concentration shows that $\text{Pu}(\text{OH})_{4(\text{aq})}$ is the dominant species in the alkaline-to-hyperalkaline pH range. Further studies with lower GLU concentrations are needed to gain a better understanding of the processes controlling the effect of the order of addition in cement radionuclide-organic systems. Experiments over a significantly longer period of time are planned to increase the relevance of these assessments for use in repository planning. In addition, experiments should be performed in the other degradation stages of HCP to understand the impact of GLU on the long-term safety of a radioactive waste repository.

Data availability statement

The original contributions presented in the study are included in the article/Supplementary Material; further inquiries can be directed to the corresponding authors.

Author contributions

JS: formal analysis, investigation, visualization, writing—original draft, and writing—review & editing. SA: conceptualization, formal analysis, writing—review & editing, investigation, and visualization. VH: investigation. DP: investigation. TR: conceptualization, formal analysis, writing—review & editing, and supervision.

References

Adam, N., Hinz, K., Gaona, X., Panak, P. J., and Altmaier, M. (2021). Impact of selected cement additives and model compounds on the solubility of Nd(III), Th(IV) and U(VI): screening experiments in alkaline NaCl, MgCl_2 and CaCl_2 solutions at elevated ionic strength. *Radiochim. Acta* 109, 431–443. doi:10.1515/ract-2021-1010

Funding

The authors declare financial support was received for the research, authorship, and/or publication of this article. This work was financially supported within the EURAD project—WP CORI, which receives funding from the EU Horizon 2020 Research and Innovation Programme under grant agreement no. 847593 and the GRaZ project by the Federal Ministry for Economic Affairs and Energy (BMWi) under contract no. 02E11415A and the Federal Ministry for the Environment, Nature Conservation, Nuclear Safety and Consumer Protection (BMUV) under contract no. 02E11860A.

Acknowledgments

The authors thank three reviewers for their helpful comments for improving the manuscript. The authors are grateful to the ESRF for granting access to synchrotron beam time. Additionally, they thank the ROBL Group from the Helmholtz-Zentrum Dresden-Rossendorf (Germany) for providing experimental support during the XANES and EXAFS measurements. The authors thank Carl-Christian Meyer and Daniel Hagenlocher for their support with the XAFS measurements, Nora Groschopf (Institute of Geosciences, Mainz) for the XRF measurements, Janik Lohmann for ICP-MS SemiQuant analysis, and Markus Breckheimer for sorption modeling.

Conflict of interest

The authors declare that the research was conducted in the absence of any commercial or financial relationships that could be construed as a potential conflict of interest.

Publisher's note

All claims expressed in this article are solely those of the authors and do not necessarily represent those of their affiliated organizations, or those of the publisher, the editors, and the reviewers. Any product that may be evaluated in this article, or claim that may be made by its manufacturer, is not guaranteed or endorsed by the publisher.

Supplementary material

The Supplementary Material for this article can be found online at: <https://www.frontiersin.org/articles/10.3389/fnuen.2023.1268767/full#supplementary-material>

Altmaier, M., Blin, V., Garcia, D., Henocq, P., Missana, T., and Ricard, D. (2021). Final version as of 19.05.2021 of deliverable D3.1 of the HORIZON 2020 project EURAD. EC Grant agreement no: 847593. State-of the art report on cement-organic-radionuclide interactions.

- Amayri, S., Fröhlich, D. R., Kaplan, U., Trautmann, N., and Reich, T. (2016). Distribution coefficients for the sorption of Th, U, Np, Pu, and Am on Opalinus Clay. *Radiochim. Acta* 104, 33–40. doi:10.1515/ract-2015-2409
- Androniuk, I., Landesman, C., Henocq, P., and Kalinichev, A. G. (2017). Adsorption of gluconate and uranyl on C-S-H phases: combination of wet chemistry experiments and molecular dynamics simulations for the binary systems. *Phys. Chem. Earth* 99, 194–203. doi:10.1016/j.pce.2017.05.005
- Böszörményi, É., Lado, J., Dudás, C., Kutus, B., Szabados, M., Varga, G., et al. (2020). The structure and composition of solid complexes comprising of Nd(III), Ca(II) and D-gluconate isolated from solutions relevant to radioactive waste disposal. *Pure Appl. Chem.* 92, 1709–1715. doi:10.1515/pac-2019-1010
- Chiorescu, I., Kremleva, A., and Krüger, S. (2022). On the sorption mode of U(IV) at calcium silicate hydrate: a comparison of adsorption, absorption in the interlayer, and incorporation by means of density functional calculations. *Minerals* 12, 1541. doi:10.3390/min12121541
- Cohen, D. (1961). The absorption spectra of plutonium ions in perchloric acid solutions. *J. Inorg. Nucl. Chem.* 18, 211–218. doi:10.1016/0022-1902(61)80390-4
- Colàs, E., Grivé, M., Rojo, I., and Duro, L. (2013). The effect of gluconate and EDTA on thorium solubility under simulated cement porewater conditions. *J. Solut. Chem.* 42, 1680–1690. doi:10.1007/s10953-013-0054-2
- Conradson, S. D., Abney, K. D., Begg, B. D., Brady, E. D., Clark, D. L., Den Auwer, C., et al. (2004). Higher order speciation effects on plutonium L_{2,3} X-ray absorption near edge spectra. *Inorg. Chem.* 43, 116–131. doi:10.1021/ic0346477
- Dario, M., Molera, M., and Allard, B. (2006). Sorption of europium on TiO₂ and cement at high pH in the presence of organic ligands. *J. Radioanal. Nucl. Chem.* 270, 495–505. doi:10.1007/s10967-006-0455-4
- Dettmann, S., Huittinen, N. M., Jahn, N., Kretzschmar, J., Kumke, M. U., Kutyma, T., et al. (2023). Influence of gluconate on the retention of Eu(III), Am(III), Th(IV), Pu(IV), and U(VI) by C-S-H (C/S = 0.8). *Front. Nucl. Eng.* 2. doi:10.3389/fnuen.2023.1124856
- DIN, (2009). Prüfverfahren für Zement in Teil 3: Bestimmung der Erstarrungszeiten und der Raumbeständigkeit, *Deutsche Fassung EN 196-3:2005+a1:2008*. Dtsch. Fass. EN DIN EN 196-3.
- Duquette, D. J., Latanision, R. M., Di Bella, C. A., and Kirstein, B. E. (2009). Corrosion issues related to disposal of high-level nuclear waste in the Yucca Mountain repository—peer reviewers' perspective. *Corrosion* 65, 272–280. doi:10.5006/1.3319133
- Duro, L., Altmaier, M., Holt, E., Mäder, U., Claret, F., Grambow, B., et al. (2020). Contribution of the results of the CEBAMA project to decrease uncertainties in the Safety Case and Performance Assessment of radioactive waste repositories. *Appl. Geochem.* 112, 104479. doi:10.1016/j.apgeochem.2019.104479
- Duro, L., Domènech, C., Grivé, M., Roman-Ross, G., Bruno, J., and Källström, K. (2014). Assessment of the evolution of the redox conditions in a low and intermediate level nuclear waste repository (SFR1, Sweden). *Appl. Geochem.* 49, 192–205. doi:10.1016/j.apgeochem.2014.04.015
- Fanghänel, T., Neck, V., and Kim, J. I. (1996). The ion product of H₂O, dissociation constants of H₂CO₃ and Pitzer parameters in the system Na⁺/H⁺/OH⁻/HCO₃⁻/CO₃²⁻/ClO₄⁻/H₂O at 25°C. *J. Solut. Chem.* 25, 327–343. doi:10.1007/bf00972890
- Gaona, X., Dähn, R., Tits, J., Scheinost, A. C., and Wieland, E. (2011). Uptake of Np(IV) by C-S-H phases and cement paste: an EXAFS study. *Environ. Sci. Technol.* 45, 8765–8771. doi:10.1021/es2012897
- Gaona, X., Montoya, V., Colàs, E., Grivé, M., and Duro, L. (2008). Review of the complexation of tetravalent actinides by ISA and gluconate under alkaline to hyperalkaline conditions. *J. Contam. Hydrol.* 102, 217–227. doi:10.1016/j.jconhyd.2008.09.017
- George, G. N., and Pickering, I. J. (2000). *EXAFSPAK - a suite of computer programs for analysis of X-ray absorption spectra*. Stanford Synchrotron Radiation Lightsource.
- Giffaut, E., Grivé, M., Blanc, P., Vieillard, P., Colàs, E., Gailhanou, H., et al. (2014). Andra thermodynamic database for performance assessment: ThermoChimie. *Appl. Geochem.* 49, 225–236. doi:10.1016/j.apgeochem.2014.05.007
- Glaus, M. A., Laube, A., and Van Loon, L. R. (2006). Solid-liquid distribution of selected concrete admixtures in hardened cement pastes. *Waste Manag.* 26, 741–751. doi:10.1016/j.wasman.2006.01.019
- Grenthe, I., Gaona, X., Rao, L., Plyasunov, A., Runde, W., Grambow, B., et al. (2020). *Second update on the chemical thermodynamics of uranium, neptunium, plutonium, americium and technetium*. Paris: OECD Publishing.
- Guo, X., Gin, S., and Frankel, G. S. (2020). Review of corrosion interactions between different materials relevant to disposal of high-level nuclear waste. *npj Mat. Degrad.* 4, 34. doi:10.1038/s41529-020-00140-7
- Häußler, V., Amayri, S., Beck, A., Platte, T., Stern, T. A., Vitova, T., et al. (2018). Uptake of actinides by calcium silicate hydrate (C-S-H) phases. *Appl. Geochem.* 98, 426–434. doi:10.1016/j.apgeochem.2018.08.021
- Jobmann, M., Bebiolka, A., Burlaka, V., Herold, P., Jahn, S., Lommerzhaim, A., et al. (2017). Safety assessment methodology for a German high-level waste repository in clay formations. *J. Rock Mech. Geotech. Eng.* 9, 856–876. doi:10.1016/j.jrmge.2017.05.007
- Jobmann, M., and Lommerzhaim, A. (2015). *Projekt ANSICHT - Endlagerkonzept sowie Verfüll- und Verschlusskonzept für das Endlagerstandortmodell SÜD*. DBE Technology GmbH.
- Kutus, B., Gaona, X., Pallagi, A., Pálíncó, I., Altmaier, M., and Sipos, P. (2020). Recent advances in the aqueous chemistry of the calcium(II)-gluconate system – equilibria, structure and composition of the complexes forming in neutral and in alkaline solutions. *Coord. Chem. Rev.* 417, 213337. doi:10.1016/j.ccr.2020.213337
- Lommerzhaim, A., and Jobmann, M. (2015). *Projekt ANSICHT - Endlagerkonzept sowie Verfüll- und Verschlusskonzept für das Standortmodell NORD*. DBE Technology GmbH.
- Martin, P., Grandjean, S., Valot, C., Carlot, G., Ripert, M., Blanc, P., et al. (2007). XAS study of (U_{1-x}Pu_x)O₂ solid solutions. *J. Alloys Compd.* 444, 410–414. doi:10.1016/j.jallcom.2007.01.032
- Matz, W., Schell, N., Bernhard, G., Prokert, F., Reich, T., Claußner, J., et al. (1999). ROBL—a CRG beamline for radiochemistry and materials research at the ESRF. *J. Synchrotron Radiat.* 6, 1076–1085. doi:10.1107/s0909049599010663
- Meleshyn, A. (2015). Gesellschaft für Anlagen-und Reaktorsicherheit (GRS) GmbH GRS-A-3844. Mechanisms of transformation of bentonite barriers – testing a new experimental concept
- Ochs, M., Dolder, F., and Tachi, Y. (2022). Decrease of radionuclide sorption in hydrated cement systems by organic ligands: comparative evaluation using experimental data and thermodynamic calculations for ISA/EDTA-actinide-cement systems. *Appl. Geochem.* 136, 105161. doi:10.1016/j.apgeochem.2021.105161
- Ochs, M., Mallants, D., and Wang, L. (2016). *Radionuclide and metal sorption on cement and concrete*. Springer International Publishing Switzerland.
- Pallagi, A., Bajnóczy, É. G., Canton, S. E., Bolin, T., Peintler, G., Kutus, B., et al. (2014). Multinuclear complex formation between Ca(II) and gluconate ions in hyperalkaline solutions. *Environ. Sci. Technol.* 48, 6604–6611. doi:10.1021/es501067w
- Parkhurst, D. L., and Appelo, C. A. J. (2016). PHREEQC (Version 3.3.5) - a computer program for speciation, batch-reaction, one-dimensional transport, and inverse geochemical calculations. Available: http://wwwbrr.cr.usgs.gov/projects/GWC_coupled/phreeqc/index.html, Accessed, 2023).
- Ravel, B., and Newville, M. (2005). ATHENA, ARTEMIS, HEPHAESTUS: data analysis for X-ray absorption spectroscopy using IFEFFIT. *J. Synchrotron Radiat.* 12, 537–541. doi:10.1107/s0909049505012719
- Rehr, J. J., Kas, J. J., Vila, F. D., Prange, M. P., and Jorissen, K. (2010). Parameter-free calculations of X-ray spectra with FEFF9. *Phys. Chem. Chem. Phys.* 12, 5503–5513. doi:10.1039/b926434e
- Reich, T., Reich, T. Y., Amayri, S., Drebert, J., Banik, N. L., Buda, R. A., et al. (2007). Application of XAFS spectroscopy to actinide environmental science. *AIP Conf. Proc.* 882, 179–183.
- Rojo, H., Gaona, X., Rabung, T., Polly, R., García-Gutiérrez, M., Missana, T., et al. (2021). Complexation of Nd(III)/Cm(III) with gluconate in alkaline NaCl and CaCl₂ solutions: solubility, TRLFS and DFT studies. *Appl. Geochem.* 126, 104864. doi:10.1016/j.apgeochem.2020.104864
- Scheinost, A. C., Claussner, J., Exner, J., Feig, M., Findeisen, S., Hennig, C., et al. (2021). ROBL-II at ESRF: a synchrotron toolbox for actinide research. *J. Synchrotron Radiat.* 28, 333–349. doi:10.1107/s1600577520014265
- Schmeide, K., Reich, T., Sachs, S., and Bernhard, G. (2006). Plutonium(III) complexation by humic substances studied by X-ray absorption fine structure spectroscopy. *Inorg. Chim. Acta* 359, 237–242. doi:10.1016/j.ica.2005.10.037
- Stietz, J., Amayri, S., Häußler, V., Scholze, R., and Reich, T. (2023). Uptake of actinides by hardened cement paste in high-salinity pore water. *Minerals* 2023, 13, 1380. doi:10.1016/j.ica.2005.10.037
- Tasi, A., Gaona, X., Rabung, T., Fellhauer, D., Rothe, J., Dardenne, K., et al. (2021). Plutonium retention in the isosaccharinate – cement system. *Appl. Geochem.* 126, 104862. doi:10.1016/j.apgeochem.2020.104862
- Taylor, H. F. W. (1997). *Cement chemistry*. Thomas Telford Publishing.
- Tits, J., Wieland, E., Bradbury, M. H., Eckert, P., and Schaible, A. (2002). *The uptake of Eu(III) and Th(IV) by calcite under hyperalkaline conditions*. PSI Bericht 02-03.
- Tits, J., Wieland, E., and Bradbury, M. H. (2005). The effect of isosaccharinic acid and gluconic acid on the retention of Eu(III), Am(III) and Th(IV) by calcite. *Appl. Geochem.* 20, 2082–2096. doi:10.1016/j.apgeochem.2005.07.004
- Tyupina, E. A., Kozlov, P. P., and Krupskaya, V. V. (2023). Application of cement-based materials as a component of an engineered barrier system at geological disposal facilities for radioactive waste—a review. *Energies* 16, 605. doi:10.3390/en16020605
- Wieland, E. (2014). Sorption data base for the cementitious near field of L/ILW and ILW repositories for provisional safety analyses for SGT-E2. *NAGRA Tech. Rep.*, 14–08.
- Wieland, E., Tits, J., Ulrich, A., and Bradbury, M. H. (2006). Experimental evidence for solubility limitation of the aqueous Ni(II) concentration and isotopic exchange of ⁶³Ni in cementitious systems. *Radiochim. Acta* 94, 29–36. doi:10.1524/ract.2006.94.1.29